CHEMISTRY OF MATERIALS

Article

pubs.acs.org/cm

Process Control of Atomic Layer Deposition Molybdenum Oxide Nucleation and Sulfidation to Large-Area MoS_2 Monolayers

Brent D. Keller,[†] Adam Bertuch,[‡] J. Provine,[§] Ganesh Sundaram,[‡] Nicola Ferralis,[†] and Jeffrey C. Grossman*,[†]

[†]Department of Material Science and Engineering, Massachusetts Institute of Technology, 77 Massachusetts Avenue, Cambridge, Massachusetts 02139, United States

[‡]Ultratech-CNT Inc., 130 Turner Street, Building 2, Waltham, Massachusetts 02453, United States

[§]Department of Electrical Engineering, Stanford University, 420 Via Palou, Stanford, California 94305, United States

Supporting Information

ABSTRACT: Recent advances in the field of two-dimensional (2D) transition metal dichalcogenide (TMD) materials have indicated that atomic layer deposition (ALD) of the metal oxide and subsequent sulfidation could offer a method for the synthesis of large area two-dimensional materials such as MoS_2 with excellent layer control over the entire substrate. However, growing large area oxide films by ALD with sub 1 nm nucleation coalescence remains a significant challenge, and the necessary steps are unexplored. In this work, we demonstrate the necessary process improvements required to achieve sub 1 nm nucleation control by characterization of nucleation domains formed by oxide deposition. Synthesis of the TMD MoS_2 from sulfidation of oxide deposited by both thermal ALD from $(tBuN)_2(NMe_2)_2Mo$ and O_3 and plasma enhanced ALD (PEALD) from $(tBuN)_2(NMe_2)_2Mo$ and remote O_2 plasma was performed. Large uniform MoS_2 areas were achieved by optimizing the effects of various growth process conditions and surface treatments on the ALD nucleation and growth of Mo-oxide and the postsulfidation of MoS_2. In addition to insights into the control of the oxide deposition, film chemistry analysis during a multistep sulfidation based on less toxic sulfur as compared to H_2S was performed for several temperature profiles revealing sulfur incorporation and molybdenum reduction at low temperatures but higher temperatures required for 2H crystal structure formation. The knowledge gained of the ALD, PEALD, and postsulfidation was leveraged to demonstrate tunable film thickness and centimeter-scale monolayer growth. Material quality can be studied independently of the MoS_2 layer count as demonstrated by the control of the monolayer photoluminescence intensity by the temperature ramp rate during sulfidation.

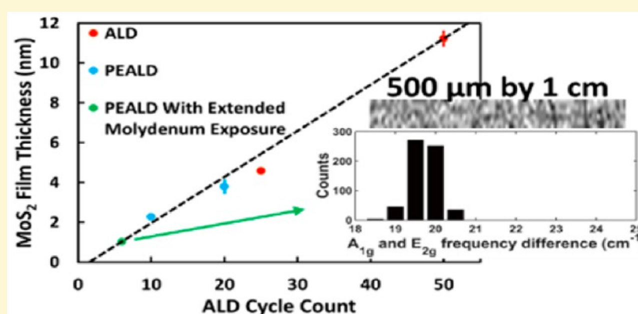

Monolayer and few layer transition metal dichalcogenides (TMDs) including MoS_2 have attracted attention as materials for transistors,[1] photovoltaics,[2,3] sensors,[4,5] and flexible systems,[6] due to their tunable[7,8] and unique electronic properties.[1,9,10] The direct technological application of such films relies on the availability of large area, high quality materials with precise layer control.[11] To date, a number of methods have been used to synthesize films of MoS_2 and other TMDs including chemical vapor deposition (CVD).[11−19] However, for applications including integrated circuits which require large area, complete and/or conformally grown films, an alternative approach under investigation for the deposition of MoS_2 and other TMDs centers around the deposition of a thin film of the transition metal or its oxide and subsequent exposure to a sulfur containing vapor at high temperature.[20,21] While this approach is limited by the uniformity, thickness, and continuity of the starting oxide or metal, for this very reason, it offers a number of potential advantages compared to CVD growth if that oxide can be deposited with exceptional control.[11,20,21] For example, extremely large area, complete films, as well as conformal monolayer coatings and abrupt vertical heterostructures may be comparatively easy to achieve. While atomic layer deposition (ALD) has been recently used to deposit extremely uniform and thin oxide films to generate large area layer control for WS_2,[22] MoS_2, and $W_xMo_{1-x}S_2$ alloys,[23] given how promising this approach is, it is surprising that it has not received much greater attention. This is in part because the oxide deposition must be highly controlled. A detailed understanding of the specific deposition conditions is required to accelerate nucleation such that film coalescence occurs at a thinner film than the amount required for a monolayer of MoS_2. This requirement is challenging even with the highly reactive precursors used for oxide synthesis[24] due to the extreme thinness of monolayer MoS_2. Previous work[23] with $Mo(CO)_6$ and oxygen plasma enhanced ALD (PEALD)

Received: September 16, 2016
Revised: February 3, 2017

ACS Publications © XXXX American Chemical Society

DOI: 10.1021/acs.chemmater.6b03951
Chem. Mater. XXXX, XXX, XXX−XXX

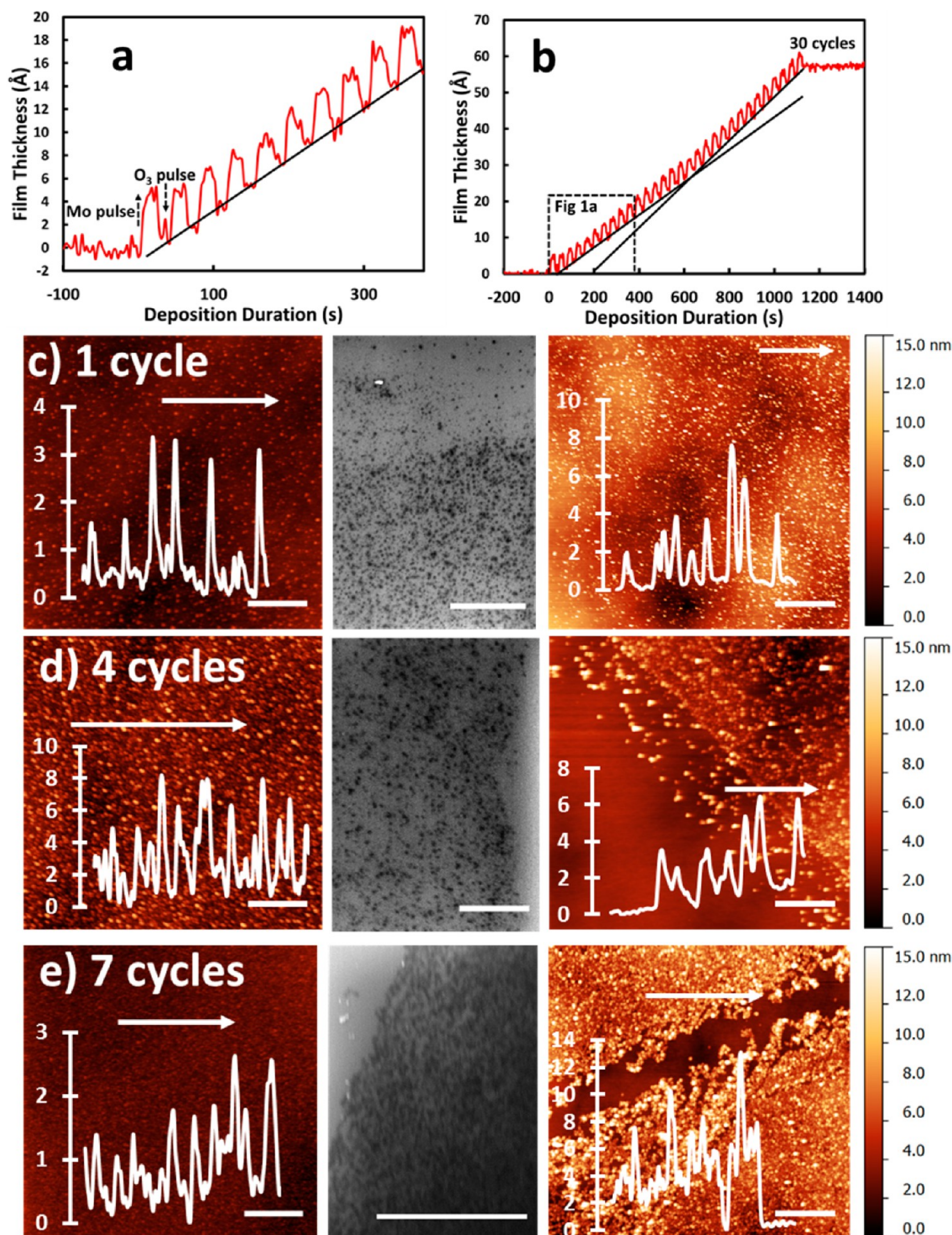

Figure 1. Nucleation of MoO_3 films from the ALD process on as received silicon wafers. (a) In situ ellipsometry of ALD growth of MoO_3 from $(NtBu)_2(NMe_2)_2Mo$ and ozone. The film can be observed to thicken with each $(NtBu)_2(NMe_2)_2Mo$ and thin following oxidation by ozone to MoO_3 with consistent growth per cycle starting after the second cycle in a true ALD process. (b) Ellipsometry of the same film deposition as in (a). The initially lower growth per cycle after approximately 15 cycles indicates nucleation inhibition in that regime. The lines in (a) and (b) are to guide the eye. (c−e) From left to right, AFM of ALD MoO_3 nucleation islands, SEM and AFM of the edge of a MoS_2 film following sulfidation and transfer to a 300 nm SiO_2 on Si wafer. The initial few nanometer islands present after 1 cycle are observed to increase in height and density as the cycle count is increased, and by 7 counts, the film nears coalescence into a few nanometers of the MoS_2 film. All scales bars, 1 μm. All AFM vertical scales are the same, and the AFM trace axis is in nanometers.

followed by sulfidation with H_2S showed promising results including excellent film uniformity and continuity. Electron mobilites in sulfidated PEALD oxides were reported in the polycrystalline WS_2 monolayer film as high as 3.9 $cm^2/(V\ s)$.[22] While this method clearly shows significant promise for large area, well controlled growth, the factors which control the

DOI: 10.1021/acs.chemmater.6b03951
Chem. Mater. XXXX, XXX, XXX−XXX

nucleation regime and thus the thickness of a coalesced oxide film are still not yet completely understood, hence limiting the applicability of this method for ultimate commercial and laboratory fabrication of MoS_2 and other TMDs.

Although sulfidation of oxides deposited by other methods has been studied extensively[11,20−22,25−28] and different recipes developed, most have converged on slow ramps[28] or multiple stage annealing[25] with high final temperatures of 800 to 1000 °C.[11] Given the thinness of the oxide films, it is surprising that such elevated temperatures are required to incorporate sufficient sulfur or other chalcogen. In addition, CVD approaches are performed over the range of 450 to 850 °C[29] and often perform better at lower temperatures where multilayer nucleation is inhibited.[15,30] In this work, we also study the chemistry of the films after lower temperature single or two stage anneals to study the evolution of the film and deduce the importance of higher temperature in the sulfidation approach.

Herein, we focus on the investigation of sulfidation of MoO_3 films deposited from bis(*tert*-butylimido)bis(dimethylamido)-molybdenum, $(^tBuN)_2(NMe_2)_2Mo$, and ozone[31] and from $(^tBuN)_2(NMe_2)_2Mo$ with remote oxygen plasma.[32] For both cases, a postsulfidation process using elemental sulfur vapor was employed. Although MoO_3 synthesized by these methods had been previously shown to have a broad ALD temperature range and high purity,[31,32] any initial nucleation regime and synthesis of ultrathin films (<1 nm) had not been explored in detail. In this work, the ALD and PEALD nucleation regime and its impact on ultrathin films of MoS_2 were studied by atomic force microscopy (AFM), scanning electron microscopy (SEM), and ellipsometry. Optimization methods to control nucleation kinetics of MoO_3 including the effect of plasma introduction, PEALD temperature, an extended Mo precursor exposure, and plasma and piranha surface pretreatments were studied. Ultimately, excellent control of the oxide nucleation was achieved to synthesize large area (>1 cm^2) monolayer MoS_2 films.

Following oxide deposition, films were sulfidated and the composition and chemistry of the film was characterized by X-ray photoelectron spectroscopy (XPS). By studying the chemistry of the films during sulfidations with multiple temperature stages to prevent volatile MoO_x loss as developed elsewhere,[25,33] insight into the further role of each stage was observed. Specifically, sulfur is observed to incorporate in S/Mo ratios of up to ∼1.4 at temperatures as high as 700 °C, but higher temperatures are still required to activate the conversion to the 2H crystal structure and grow the grain size (as shown by Raman) and to achieve stoichiometric S incorporation. Finally, through slower sulfidation temperature ramps, the photoluminescence (PL) intensity and the 2H MoS_2 crystal quality could be improved, independent of the layer control provided by the PEALD nucleation engineering.

EXPERIMENTAL SECTION

Oxide Deposition. The MoO_3 films were deposited using both thermal ALD and PE-ALD techniques. The thermal ALD process was conducted in a cross-flow, hot wall Ultratech-Cambridge Nanotech Savannah system at 300 °C. The $(NtBu)_2(NMe_2)_2Mo$ precursor was delivered to the chamber using a boosted N_2 precursor delivery. The ozone coreactant was delivered to the chamber with an O_2/O_3 flow rate of 330 sccm and a concentration of 120 mg/L. The deposition was performed as described by Bertuch et al.[31] The PEALD depositions were performed at 150 °C in a top flow reactor (Ultratech-CNT Fiji system) using a remote inductively coupled plasma (ICP) unit. The argon gas flow for the process was 20 sccm of Ar carrier gas with 200 sccm of plasma Ar continuously flowing through the chamber. The Mo precursor and delivery technique was unchanged and utilized the boosted precursor delivery technique with Ar instead of N_2 gas. The coreactant was O_2 plasma generated at 300 W in a flowing gas of 20 sccm O_2 and 80 sccm Ar. Plasma exposure times were 20 s with a purge time of 5 s. For extended Mo precursor exposure, the downstream vacuum valve was closed for 14 s during the precursor pulse step and then opened for the precursor purge and plasma steps. The piranha treatment was performed using 3 parts 98% H_2SO_4 and 1 part 30% H_2O_2 within 4 h of the MoO_3 film deposition. *(CAUTION: "Piranha" solution reacts violently with organic materials; it must be handled with extreme care.)*

Sulfidation. Sulfidations were performed at 240 mTorr with 45 sccm of argon and 4 sccm of H_2 gas flowing in a 1 in. diameter quartz tube. Solid sulfur (500 mg) was supplied at either 125 or 135 °C immediately upstream of the heater. Samples were placed parallel to the direction of gas flow. No effect on the sulfidation was observed for the variation in sulfur source temperature. For multistage sulfidations, temperature ramp times between stages were 10 min, and the temperature was held at each step for 30 min unless otherwise mentioned.

Film Transfer. Following sulfidation, films were transferred to fresh 300 nm SiO_2 on Si wafer fragments to provide clean edges for AFM characterization. Films were coated with ebeam resist (MicroChem A5) and floated on 10% HF to remove native or thermal oxide layer below the MoS_2. Upon release of the polymer film, films were scooped with a glass slide and floated on rinse solutions of DI water before being picked up with the target wafer fragment and dried at 80 °C. Warm acetone was used to remove the polymer film.

Characterization. X-ray photoluminescence spectroscopy was performed over regions 400 μm in diameter using a Thermo Scientific K-Alpha XPS with Al Kα radiation. XPS peak deconvolution was performed using Casa XPS with Shirley backgrounds subtracted and Gaussian-Lorentzian product line shapes with 90% Lorentzian weighting. Micro-Raman spectra were acquired using a Horiba LabRAM 800 HR spectrometer equipped with a 514.5 nm excitation source. The laser spot on the sample was ∼800 nm in diameter and had a power of ∼4 mW at the sample surface. AFM was performed using a Veeco Metrology Nanoscope IV Scanned Probe Microscope Controller with Dimension 3100 SPM in tapping mode with PPP-NCHR probes. SEM was performed on a Zeiss Ultra55 operated at 5 kV.

RESULTS AND DISCUSSION

ALD and PEALD of MoO_3 films were deposited on silicon wafers with both native oxide and thermal oxide (300 nm) surfaces. The ALD process was monitored with *in situ* ellipsometry (Figure 1a). The deposition is observed to be stepwise in a true ALD process with film thickness controlled by cycle count. The growth per cycle (GPC) was observed to be constant after approximately 15 cycles indicating a nucleation inhibited regime in the first 15 cycles. AFM of the as deposited oxide (Figure 1b−d) shows nucleation islands after the first cycle which can be observed to increase in size and density through the fourth and seventh cycles. Following sulfidation, MoS_2 was transferred onto fresh thermal oxide (300 nm) on silicon wafers using a polymer transfer; MoS_2 films were coated with PMMA, followed by etching of the underlying native oxide or thermal oxide with 10% HF, rinsed with DI water, and transferred to the new substrate, and the PMMA was removed with warm acetone. Scanning electron microscopy (SEM) and AFM of the edges of transferred MoS_2 show that the nucleation islands are preserved resulting in an incomplete and rough film (Figure 1b−d). While the PMMA transfer is possible with even the very thin native oxide, at high temperatures, silicon and sulfur react and form volatile

DOI: 10.1021/acs.chemmater.6b03951
Chem. Mater. XXXX, XXX, XXX−XXX

products,[34,35] and thus, without the protective diffusion barrier of a thick thermal oxide, the sulfur vapors were observed to etch pits in silicon wafers at temperatures above 700 °C (Figure S1).

Because the film morphology was preserved during sulfidation (Figure 1b−d), to grow complete monolayer MoS_2 over large areas, the coalesced oxide film thickness must be reduced to less than that required to produce a monolayer of MoS_2 from MoO_3 (assuming no losses of Mo due to volatility or diffusion during the sulfidation and based on the bulk densities of MoO_3 and MoS_2, approximately 0.7 nm thick). To reduce the thickness of a film at coalescence, the density of nucleation islands must be increased. This can be accomplished through increasing precursor reactivity and dosing or by reducing surface mobility of adhered species, if they are sufficiently mobile to diffuse to nucleation islands. To increase reactivity, the process was adapted to PEALD. While thermal ALD deposited films were grown at 300 °C to provide the highest purity film,[31] higher temperatures lead to larger nucleation islands due to increased ad-species diffusivity and/or run-away CVD growth. Because of the increased reactivity of PEALD, the temperature can be reduced without sacrificing film purity (Figure S2). Figure 2 shows >10 nm films deposited by PEALD at 150, 200, and 300 °C. At 300 °C, very large nucleation islands are observed, indicative of precursor decomposition and CVD growth at nucleation sites spaced hundreds of nanometers apart. The roughness of the films is dramatically reduced at lower temperature indicating a true ALD process and is further improved from 200 to 150 °C with reduced surface mobility of precursor species.

Nucleation islands with one nanometer thickness are still observed for PEALD growth at 150 °C (Figure 3a). While significantly improved over the ALD process after a similar number of cycles, the islands are still larger than needed to produce monolayer MoS_2 from coalesced films. In an attempt to further increase the nucleation density (and thus reduce coalesced film thickness), the number of molybdenum precursor pulses was increased, but no qualitative improvement in the nucleation regime was observed (Figure 3b) indicating that Mo precursor transport and reaction kinetics are not limiting in the nucleation process. Large nucleation features associated with surface contaminants not removed by an oxygen plasma treatment were exacerbated by the extended molybdenum exposure.

Finally, a piranha cleaning treatment prior to PEALD growth was found to be exceptionally effective in increasing nucleation density and eliminating nucleation islands larger than 1 nm after 5 cycles (Figure 3c). The piranha treatment increases the hydrophilicity of the surface, and a high density of hydrophilic functional groups often improves ALD nucleation. However, piranha followed by an oxygen plasma cleaning immediately before PEALD growth did not improve nucleation density, highlighting the importance of hydroxyl functionalities left by the piranha etch for reaction with the molybdenum precursor (Figure 3d) as opposed to a cleaning or hydrophilicity effect which would be largely preserved under the oxygen plasma. To further highlight this distinction, piranha was also effective in reducing the size of the large nucleation islands likely related to contamination, and this effect was preserved after an additional oxygen plasma cleaning.

To sulfidate the oxide films into MoS_2, approximately 1 cm^2 wafer cuttings were loaded into a quartz tube furnace under an Ar and H_2 atmosphere at low pressure. At the desired temperature, a solid sulfur source immediately upstream of the furnace was heated to produce sulfur vapors. Because MoO_3 is a volatile oxide, a multistep sulfidation was adopted, to first partially reduce or sulfidate the film at lower temperature (500 to 800 °C) before final processing at higher temperature.[23,25] Figure 4a shows Mo 3d XPS for several annealing temperatures. The as-deposited oxides show a single doublet at higher binding energy as expected for Mo^{6+}. Peak broadening is indicative of moderate contribution from lower oxidation states. This is in contrast to previous sulfidation work by Song et al.[23] which started from a less oxidized film deposited using a $Mo(CO)_6$ precursor with a single broad Mo 3d complex showing large contributions from Mo^{6+}, Mo^{5+}, and Mo^{4+}.

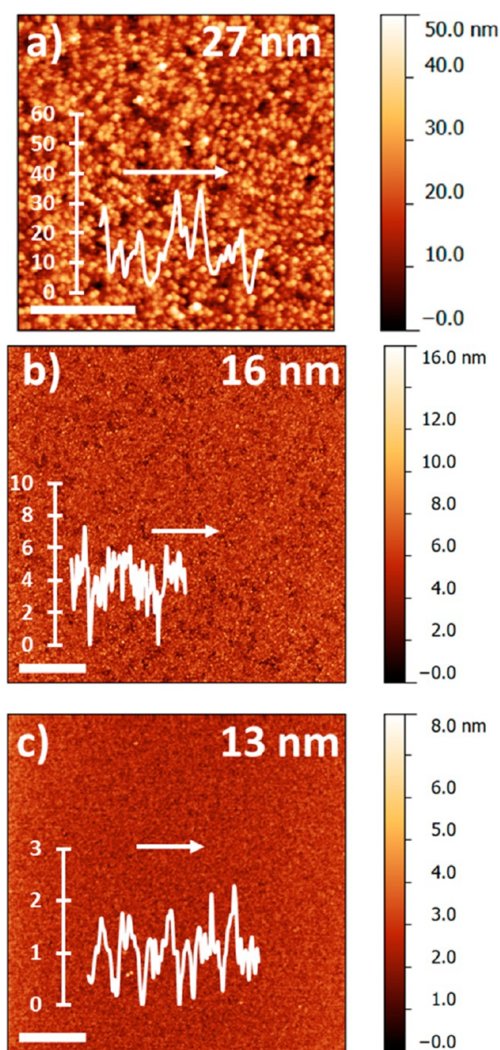

Figure 2. Impact of temperature on the PEALD process. AFM images of thick films showing rough large nucleation features at (a) 300 °C and coalesced films at (b) 200 and (c) 150 °C indicating a transition in growth regime. The 150 °C samples are observed to be smoother than the 200 °C samples indicating the reduced mobility of active species at lower temperature. All scale bars, 1 μm. AFM trace axis is in nanometers.

It would be expected that sulfur incorporation would be very rapid due to the extreme thinness of the film and even moderately elevated temperatures. However, after processing at 300 °C, we observe only partial reduction with Mo^{6+}, Mo^{5+}, and Mo^{4+}, all present and with 37 atomic percentage (at %) sulfur based on deconvolution of the Mo 3d 5/2 and sulfur 2s complex (Figure 4b). It should be noted that given the small

DOI: 10.1021/acs.chemmater.6b03951
Chem. Mater. XXXX, XXX, XXX−XXX

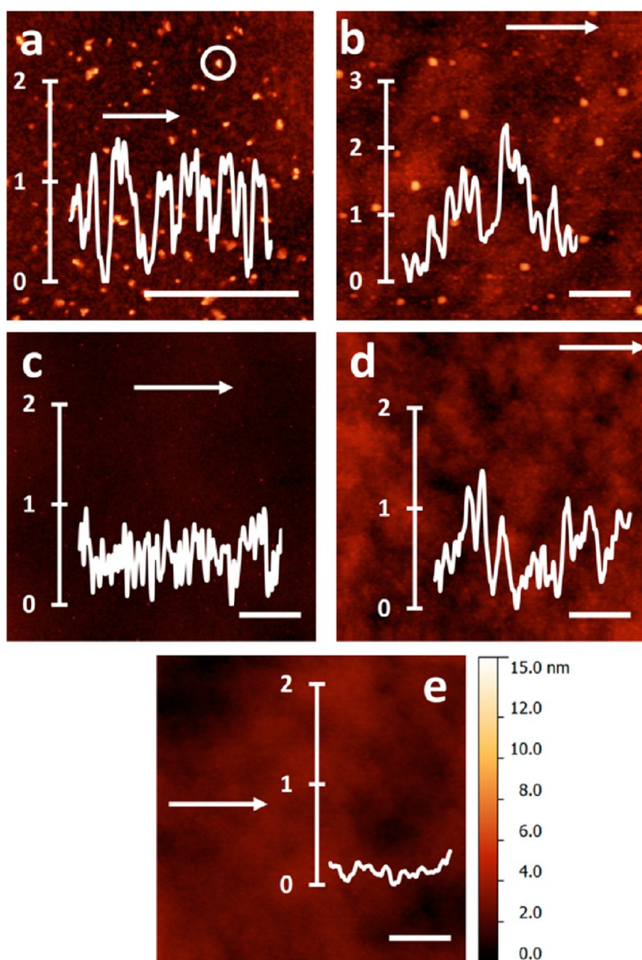

Figure 3. Control of MoO_3 nucleation. (a) AFM of 5 cycle PEALD deposited MoO_3 following 4 min of oxygen plasma clean. Large features (e.g., feature inside white circle) are likely sources of nucleation from remaining surface contaminants, and small nucleation features can be seen covering the remainder of the surface. The trace from a clean region (white arrow) shows these smaller nucleation features are ≥1 nm which result in multilayer MoS_2. (b) 5 cycles of PEALD with addition of a 14 s $(NtBu)_2(NMe_2)_2Mo$ extended exposure on a similar oxygen plasma cleaned wafer. Nucleation islands remain in the ≥1 nm regime. (c) 6 cycle PEALD deposited MoO_3 following a piranha cleaning without a plasma cleaning. The piranha cleaning removes larger surface contaminants, and nucleation islands are observed to be <1 nm in height which is critical to large area monolayer MoS_2 fabrication. (d) 5 cycle PEALD deposited MoO_3 following a piranha cleaning but with a subsequent oxygen plasma cleaning. Greater than 1 nm tall nucleation islands, which were eliminated with the piranha treatment, are again observed when the piranha treated sample is exposed to oxygen plasma. The larger features likely related to contamination removed by piranha are still surpressed. (e) As received wafer for comparison. All scales bars, 1 μm. All AFM vertical scales are the same, and AFM trace axis is in nanometers.

difference in Mo 3d binding energy in MoO_2 and MoS_2 (approximately 0.2 eV)[36,37] it is possible the reduced Mo is present as a sulfide, oxide, or combined structure. Increasing the temperature to 600 °C increases the sulfur content (58 at % sulfur), but the film remains very sulfur poor; elevating the second step temperature to 700 °C does not result in significant further sulfidation (59 at % sulfur). S 2p XPS (Figure 4c) shows that the initial sulfur incorporation lacks chemical uniformity

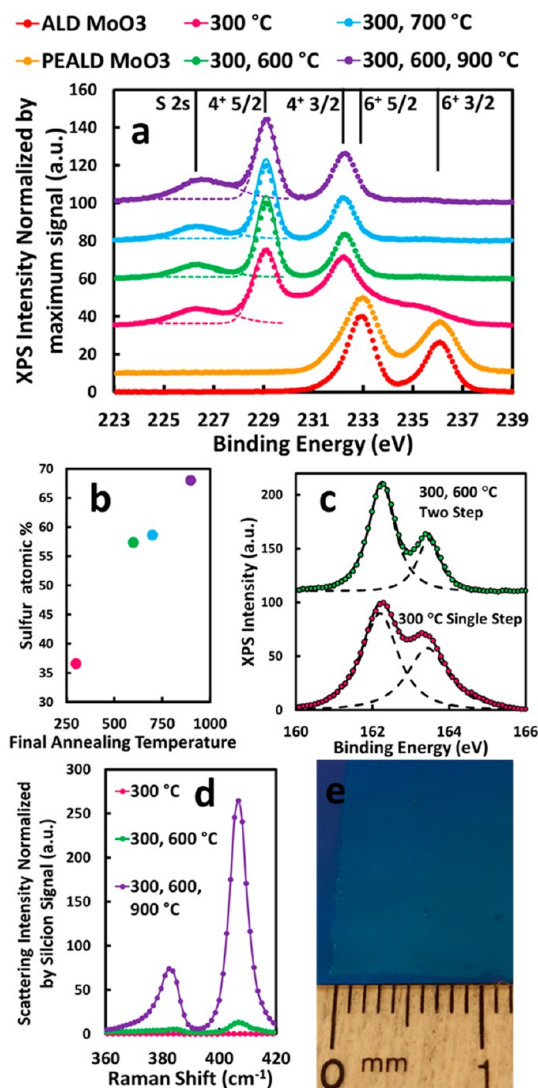

Figure 4. Multistep sulfidation of (a) Mo 3d XPS normalized by maximum signal for as deposited ALD and PEALD films and following single step processing at 300 °C, 2 step processing first at 300 °C and then at 600 or 700 °C, and 3 step processing at 300, 600, then 900 °C. Partial reduction is observed at 300 °C (downshift of Mo 3d 3/2 and 5/2 and appearance of S 2s at 226 eV). Films annealed at about 600 °C show complete reduction of molybdenum. For the annealed samples, the S 2s and Mo^{4+} 3d 5/2 signals were deconvoluted to determine the sulfur content. Dashed lines represent fitted contributions of S 2s and Mo^{4+} 3d 5/2, and the solid line represents total contribution. (b) Atomic percentage of sulfur based on the Mo 3d and S 2s peaks showing partial incorporation of sulfur during a 300 °C single step anneal and final stoichiometric incorporation via a three step anneal. (c) S 2p XPS initially has broad peaks at 300 °C indicating disorder and poor uniformity in a chemical environment. By 600 °C in a two step anneal, peaks are sharp and agree well with the literature[36−41] (binding energies of 162.2 eV for S $2p_{3/2}$ and 163.5 for eV $2p_{1/2}$ respectively). Dashed lines indicate fits for the $2p_{3/2}$ and $2p_{1/2}$. Solid lines represent the sum of the fits. As the sulfur content increases at higher temperature, Raman spectra (d) show the emergence in the A_{1g} and E_{2g} peaks characteristic of the 2H structure of multilayer MoS_2. Processing up to 900 °C shows a dramatic increase in the intensity of these peaks. (e) Optical image of 4.5 nm thick MoS_2 following transfer to a larger 300 nm SiO_2 on Si substrate showing centimeter scale uniformity achieved with ALD and the postsulfidation process. Few small tears in the film likely caused by regions of poor adhesion during transfer.

DOI: 10.1021/acs.chemmater.6b03951
Chem. Mater. XXXX, XXX, XXX−XXX

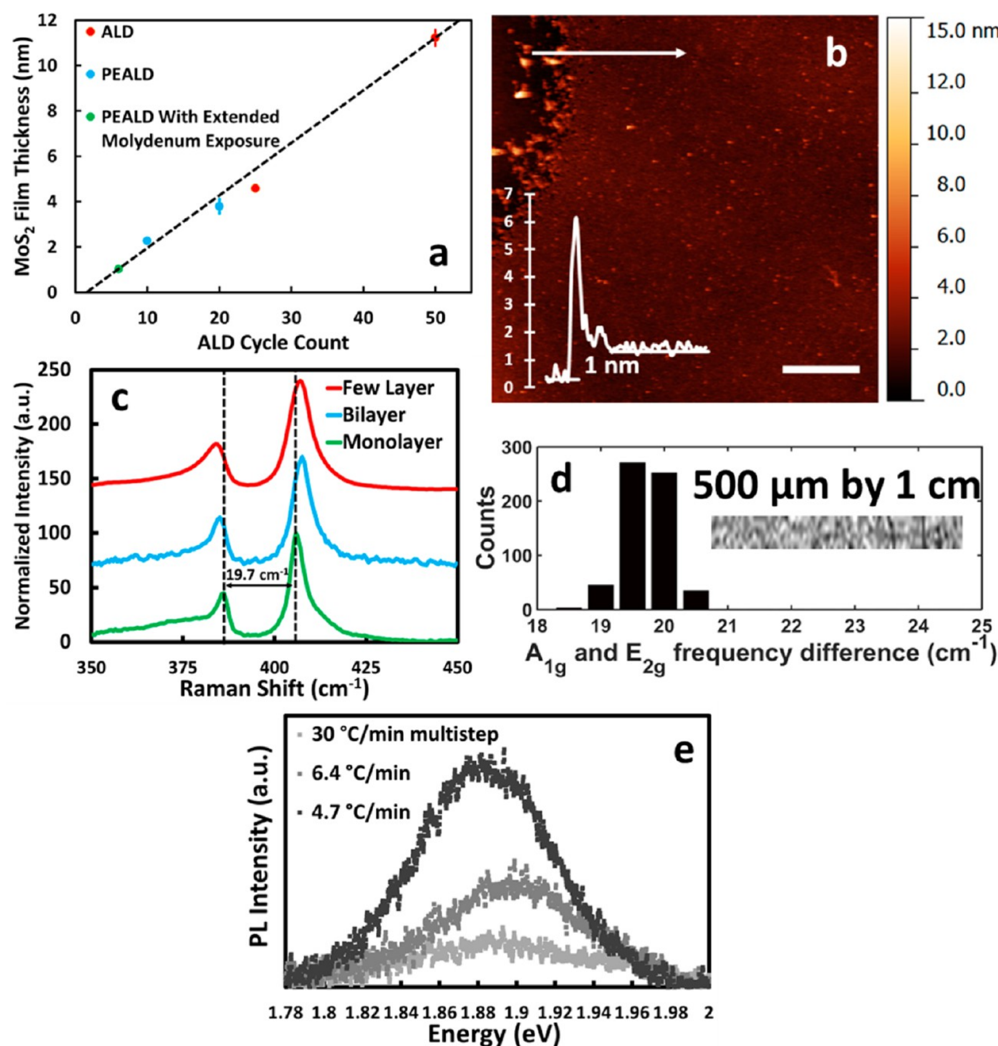

Figure 5. MoS_2 layer control. (a) Resulting MoS_2 film thickness as a function of the ALD or PEALD cycle count down to the monolayer regime. Line is only to guide the eye. (b) AFM of monolayer MoS_2 with a trace showing ∼1 nm film thickness. Scale bar, 1 μm. (c) Raman spectroscopy of monolayer, bilayer, and few layer MoS_2 samples based on E_{2g} and A_{1g} peak separation. (d) Large area Raman mapping of monolayer MoS_2 showing film uniformity on the centimeter scale. Histogram shows a single distribution of peak spacing centered between 19.5 and 20 cm^{-1} and with a width of the detector resolution of approximately 0.5 cm^{-1}. Inset shows spatial map indicating variation is random across the sample and uniformity in thickness. (e) Effect of heating rate on PL signal intensity for monolayer MoS_2 samples sulfurized for 30 min at a 300 °C hold and then a 30 °C/min ramp with additional holds for 10 min at 600 and 1000 °C (multistep) as well as two samples with linear temperature profiles (no holds) from 300 to 1000 °C.

with broad peaks fitting the $2p_{3/2}$ and $2p_{1/2}$. However, although the film remains sulfur poor, by 600 °C, the S 2p XPS shows narrow peaks and agreement with the literature[36−41] for MoS_2 (binding energies of 162.2 and 163.5 eV for S $2p_{3/2}$ and $2p_{1/2}$, respectively).

After the 300 °C single step sulfidation, no Raman signal associated with 2H MoS_2 is present (Figure 4c) suggesting that the material remains amorphous at these temperatures. This agrees well with broad S 2p XPS peaks and several oxidation states of Mo (including any from residual oxide) observed after this single step anneal. After the second annealing step at 600 °C when the reduction of molybdenum to Mo^{4+} is complete and the S 2p XPS is sharpened, a weak Raman signal emerges in the film. Since the film remains depleted in sulfur and the Raman response is weak (Figure 4d), it is likely still mostly amorphous or in extremely small grained crystal domains. To achieve a stoichiometric film and improve the crystallinity, a third step was added to the anneal at 900 and 1000 °C, both resulting in a dramatic increase in the Raman scattering intensity and an increase in sulfur content to a nearly stoichiometric 68 at % sulfur (Figure 4b,d). From these results, we conclude that, even though Mo reduction and sulfur incorporation proceeds at lower temperatures up to approximately 60 at % sulfur, a large barrier to conversion to the 2H crystal structure and growth of its grains requires temperatures of 900 °C or higher to activate the conversion and achieve stoichiometric films.

Following sulfidation, films were transferred to new Si wafers with 300 nm of thermal oxide to illustrate the uniformity and measure thickness by AFM. With the exception of small tears and wrinkles associated with the polymer transfer, the MoS_2 films prepared by this method show excellent uniformity with complete MoS_2 coverage of the sulfidated wafer fragment (Figure 4e). Figure 5a shows postsulfidation thickness as a function of cycle count for several materials as measured by AFM as well as the oxide thickness for ALD deposited films

DOI: 10.1021/acs.chemmater.6b03951
Chem. Mater. XXXX, XXX, XXX−XXX

measured by ellipsometry. The method demonstrates broad control over the thickness of large area MoS_2 films, from monolayer through several nanometers. The positive x-intercept of the guideline shows the combined effects of the remaining nucleation delay and volatile losses during sulfidation. Raman spectra for transferred films show the expected difference in Raman shifts between the A_{1g} and E_{2g} bands (23.6, 22.5, and 19.7 cm^{-1}, respectively) for multi, bi-, and monolayer. In particular, a difference of less than 20 cm^{-1} (Figure 5b) was found for the monolayer film which agrees with values reported elsewhere for monolayer MoS_2 on SiO_2 (19 to 20.6 cm^{-1}).[23,33,42] AFM characterization shows approximately one nanometer thick film, which is slightly thicker than the bulk layer spacing (0.7 nm), probably due to layer substrate interactions, in agreement with monolayer MoS_2 reported elsewhere.[23,43] Finally, to demonstrate the uniformity of an ALD based approach to MoS_2 growth, Raman spectra were sampled across a 500 μm by 1 cm region with 100 μm distances between points (Figure 5d) for a monolayer MoS_2 sample prepared with a 1000 °C final annealing step. The hundreds of spectra collected indicate a single distribution in A_{1g} and E_{2g} centered at ~19.7 cm^{-1} and are width limited by the frequency resolution of the detector (0.5 cm^{-1}).

PL at the direct band gap energy (1.8 to 1.9 eV)[7,8] indicates high crystal quality[44,45] monolayer MoS_2. PL spectra were collected for MoS_2 monolayer films following sulfidation. While the ALD process sets the number of layers of MoS_2 as shown above, the crystal domain size is determined by the kinetics of the nucleation and growth of the 2H crystal structure. The decoupling of layer control from crystal quality is an advantage which can allow for independent progress on both challenges. To demonstrate that this approach is possible, we explore the effect of sulfidation temperature ramp rate on this 2H nucleation and growth process, and to improve the crystal quality of the material as determined by PL, samples with an accelerated multistep sulfidation (30 °C/min and holds for 10 min at 600 and 1000 °C) and with slow but linear temperature profiles (4.7 and 6.4 °C/min up to 1000 °C) were prepared. All samples were first partially reduced and sulfidated at 300 °C for 30 min. The slower ramp rate samples show much stronger PL emission which indicates larger and/or more defect free 2H crystal domains. Crystal domain size is determined by the competition of crystal growth from the amorphous MoS_x matrix and nucleation of new crystal domains in that matrix. By heating more gradually, the nucleation rate is comparatively suppressed and 2H MoS_2 domains grow much larger before encountering other domains. This illustrates the potential to leverage the excellent layer control demonstrated here with future progress around substrate epitaxy or other control of high temperature 2H TMD grain formation/growth to achieve truly high quality MoS_2, layer controlled, complete film, and large or single crystal domains.

In conclusion, detailed nucleation engineering of the metal oxide film led to the successful growth of large scale, uniform thickness controlled MoS_2 films via sulfidation of ALD and PEALD Mo-oxide films. The effect of temperature, a 14 s extended precursor exposure, and plasma and piranha surface treatment on MoO_3 PEALD deposition were studied. Plasma processing at 150 °C was found to be beneficial to nucleation, and a piranha treated surface immediately preceding the first ALD pulse was critical to monolayer MoS_2 fabrication. The molybdenum chemistry and sulfur incorporation were also studied at each stage of the subsequent multistep sulfidation. Although molybdenum reduction and sulfur incorporation into the films occurred at temperatures below 700 °C, elevation to 900 °C was required to activate the conversion to crystallize the 2H structure. Through the control of the nucleation process, centimeter scale monolayers with uniformity across the substrate were synthesized as demonstrated by AFM and Raman spectroscopies.

Ultimately, any growth method for MoS_2 or other TMDs for applications such as digital logic must offer three features: layer uniformity, complete or controlled coverage, and large domain size or preferably single crystallinity. One of the key advantages of the method presented is the decoupling of the MoS_2 crystallinity from layer control and coverage by separating this into two distinct nucleation processes. Specifically, we have shown that, through control of the ALD process, the nucleation density of the oxide can be controlled on the wafer scale to provide two of the three key features, layer control and uniformity. The subsequent nucleation of the 2H crystal structure at high temperature after sulfur incorporation independently controls the final property, crystallinity. While this will be the subject of future work, crystal quality can be approached through a number of methods including heating rate as shown here. However, the ability to tackle this last property, independent of the layer count and uniformity of the film, because it is already set by the nucleation engineering of the ALD oxide, is a significant step toward wafer scale, high quality, MoS_2.

ASSOCIATED CONTENT

Supporting Information

The Supporting Information is available free of charge on the ACS Publications website at DOI: 10.1021/acs.chemmater.6b03951.

Optical image of sulfur etching of silicon; XPS oxide composition; survey XPS spectra (PDF)

AUTHOR INFORMATION

Corresponding Author

*E-mail: jcg@mit.edu. Phone: (+1) 617-324-3566.

ORCID

Brent D. Keller: 0000-0001-8975-6434

Author Contributions

The manuscript was written through contributions of all authors. All authors have given approval to the final version of the manuscript.

Notes

The authors declare no competing financial interest.

ACKNOWLEDGMENTS

We would like to thank Federico Pinna and Patrick Yu for their assistance in performing some of the sulfidations. This work made use of the MRSEC Shared Experimental Facilities at MIT, supported by the National Science Foundation under award number DMR-1419807, and at the Center for Nanoscale Systems (CNS), a member of the National Nanotechnology Infrastructure Network (NNIN), which is supported by the National Science Foundation under NSF award no. ECS-0335765. CNS is part of Harvard University.

DOI: 10.1021/acs.chemmater.6b03951
Chem. Mater. XXXX, XXX, XXX−XXX

■ REFERENCES

(1) Radisavljevic, B.; Radenovic, A.; Brivio, J.; Giacometti, V.; Kis, A. Single-Layer MoS2 Transistors. *Nat. Nanotechnol.* **2011**, *6*, 147−150.

(2) Britnell, L.; Ribeiro, R. M.; Eckmann, A.; Jalil, R.; Belle, B. D.; Mishchenko, A.; Kim, Y.-J.; Gorbachev, R. V.; Georgiou, T.; Morozov, S. V.; Grigorenko, A. N.; Geim, A. K.; Casiraghi, C.; Castro Neto, A. H.; Novoselov, K. S. Strong Light-Matter Interactions in Heterostructures of Atomically Thin Films. *Science* **2013**, *340*, 1311−1314.

(3) Bernardi, M.; Palummo, M.; Grossman, J. C. Extraordinary Sunlight Absorption and 1 Nm-Thick Photovoltaics Using Two-Dimensional Monolayer Materials. *Nano Lett.* **2013**, *13*, 3664.

(4) Perkins, F. K.; Friedman, A. L.; Cobas, E.; Campbell, P. M.; Jernigan, G. G.; Jonker, B. T. Chemical Vapor Sensing with Monolayer MoS 2. *Nano Lett.* **2013**, *13*, 668−673.

(5) Liu, B.; Chen, L.; Liu, G.; Abbas, A. N.; Fathi, M.; Zhou, C. High-Performance Chemical Sensing Using Schottky-Contacted Chemical Vapor Deposition Grown Monolayer MoS2 Transistors. *ACS Nano* **2014**, *8*, 5304−5314.

(6) Chhowalla, M.; Shin, H. S.; Eda, G.; Li, L.-J.; Loh, K. P.; Zhang, H. The Chemistry of Two-Dimensional Layered Transition Metal Dichalcogenide Nanosheets. *Nat. Chem.* **2013**, *5*, 263−275.

(7) Splendiani, A.; Sun, L.; Zhang, Y.; Li, T.; Kim, J.; Chim, C.-Y.; Galli, G.; Wang, F. Emerging Photoluminescence in Monolayer MoS2. *Nano Lett.* **2010**, *10*, 1271−1275.

(8) Mak, K.; Lee, C.; Hone, J.; Shan, J.; Heinz, T. Atomically Thin MoS2: A New Direct-Gap Semiconductor. *Phys. Rev. Lett.* **2010**, *105*, 2−5.

(9) Zhu, H.; Wang, Y.; Xiao, J.; Liu, M.; Xiong, S.; Wong, Z. J.; Ye, Z.; Ye, Y.; Yin, X.; Zhang, X. Observation of Piezoelectricity in Free-Standing Monolayer MoS_2. *Nat. Nanotechnol.* **2015**, *10*, 151−155.

(10) Lopez-Sanchez, O.; Lembke, D.; Kayci, M.; Radenovic, A.; Kis, A. Ultrasensitive Photodetectors Based on Monolayer MoS2. *Nat. Nanotechnol.* **2013**, *8*, 497.

(11) Shi, Y.; Li, H.; Li, L.-J. Recent Advances in Controlled Synthesis of Two-Dimensional Transition Metal Dichalcogenides via Vapour Deposition Techniques. *Chem. Soc. Rev.* **2015**, *44*, 2744.

(12) Lee, Y.-H.; Yu, L.; Wang, H.; Fang, W.; Ling, X.; Shi, Y.; Lin, C.-T.; Huang, J.-K.; Chang, M.-T.; Chang, C.-S.; Dresselhaus, M. S.; Palacios, T.; Li, L.-J.; Kong, J. Synthesis and Transfer of Single Layer Transition Metal Disulfides on Diverse Surfaces. *Nano Lett.* **2013**, *13*, 1852.

(13) Lee, Y.-H.; Zhang, X.-Q.; Zhang, W.; Chang, M.-T.; Lin, C.-T.; Chang, K.-D.; Yu, Y.-C.; Wang, J. T.-W.; Chang, C.-S.; Li, L.-J.; Lin, T.-W. Synthesis of Large-Area MoS2 Atomic Layers with Chemical Vapor Deposition. *Adv. Mater.* **2012**, *24*, 2320−2325.

(14) Cong, C.; Shang, J.; Wu, X.; Cao, B.; Peimyoo, N.; Qiu, C.; Sun, L.; Yu, T. Synthesis and Optical Properties of Large-Area Single-Crystalline 2D Semiconductor WS 2 Monolayer from Chemical Vapor Deposition. *Adv. Opt. Mater.* **2014**, *2*, 131−136.

(15) Huang, J.-K.; Pu, J.; Hsu, C.-L.; Chiu, M.-H.; Juang, Z.-Y.; Chang, Y.-H.; Chang, W.-H.; Iwasa, Y.; Takenobu, T.; Li, L.-J. Large-Area Synthesis of Highly Crystalline WSe 2 Monolayers and Device Applications. *ACS Nano* **2014**, *8*, 923−930.

(16) Dumcenco, D.; Ovchinnikov, D.; Marinov, K.; Lazić, P.; Gibertini, M.; Marzari, N.; Sanchez, O. L.; Kung, Y.; Krasnozhon, D.; Chen, M.; Bertolazzi, S.; Gillet, P.; Fontcuberta i Morral, A.; Radenovic, A.; Kis, A. Large-Area Epitaxial Monolayer MoS 2. *ACS Nano* **2015**, *9*, 4611−4620.

(17) Kang, K.; Xie, S.; Huang, L.; Han, Y.; Huang, P. Y.; Mak, K. F.; Kim, C.-J.; Muller, D.; Park, J. High-Mobility Three-Atom-Thick Semiconducting Films with Wafer-Scale Homogeneity. *Nature* **2015**, *520*, 656−660.

(18) Bilgin, I.; Liu, F.; Vargas, A.; Winchester, A.; Man, M. K. L.; Upmanyu, M.; Dani, K.; Gupta, G.; Talapatra, S.; Mohite, A. D.; Kar, S. Chemical Vapor Deposition Synthesized Atomically-Thin Molybdenum Disulfide with Optoelectronic-Grade Crystalline Quality. *ACS Nano* **2015**, *9*, 8822.

(19) Yu, Y.; Li, C.; Liu, Y.; Su, L.; Zhang, Y.; Cao, L. Controlled Scalable Synthesis of Uniform, High-Quality Monolayer and Few-Layer MoS2 Films. *Sci. Rep.* **2013**, *3*, 1866.

(20) Gutiérrez, H. R.; Perea-López, N.; Elías, A. L.; Berkdemir, A.; Wang, B.; Lv, R.; López-Urías, F.; Crespi, V. H.; Terrones, H.; Terrones, M. Extraordinary Room-Temperature Photoluminescence in Triangular WS2Monolayers. *Nano Lett.* **2013**, *13*, 3447.

(21) Zhou, L.; Xu, K.; Zubair, A.; Liao, A. D.; Fang, W.; Ouyang, F.; Lee, Y. H.; Ueno, K.; Saito, R.; Palacios, T.; Kong, J.; Dresselhaus, M. S. Large-Area Synthesis of High-Quality Uniform Few-Layer $MoTe_2$. *J. Am. Chem. Soc.* **2015**, *137*, 11892−11895.

(22) Song, J.; Park, J.; Lee, W.; Choi, T.; Jung, H.; Lee, C. W.; Hwang, S.; Myoung, J. M.; Jung, J.; Kim, S.; Lansalot-matras, C.; Kim, H. *ACS Nano* **2013**, *7*, 11333−11340.

(23) Song, J.-G.; Ryu, G. H.; Lee, S. J.; Sim, S.; Lee, C. W.; Choi, T.; Jung, H.; Kim, Y.; Lee, Z.; Myoung, J.-M.; Dussarrat, C.; Lansalot-Matras, C.; Park, J.; Choi, H.; Kim, H. Controllable Synthesis of Molybdenum Tungsten Disulfide Alloy for Vertically Composition-Controlled Multilayer. *Nat. Commun.* **2015**, *6*, 7817.

(24) George, S. M. Atomic Layer Deposition: An Overview. *Chem. Rev.* **2010**, *110*, 111−131.

(25) Lin, Y.-C.; Zhang, W.; Huang, J.-K.; Liu, K.-K.; Lee, Y.-H.; Liang, C.-T.; Chu, C.-W.; Li, L.-J. Wafer-Scale MoS2 Thin Layers Prepared by MoO3 Sulfurization. *Nanoscale* **2012**, *4*, 6637.

(26) Wang, X.; Feng, H.; Wu, Y.; Jiao, L. Controlled Synthesis of Highly Crystalline MoS 2 Flakes by Chemical Vapor Deposition. *J. Am. Chem. Soc.* **2013**, *135*, 5304−5307.

(27) Lin, Y.-C.; Lu, N.; Perea-Lopez, N.; Li, J.; Lin, Z.; Peng, X.; Lee, C. H.; Sun, C.; Calderin, L.; Browning, P. N.; Bresnehan, M. S.; Kim, M. J.; Mayer, T. S.; Terrones, M.; Robinson, J. A. Direct Synthesis of van Der Waals Solids. *ACS Nano* **2014**, *8*, 3715−3723.

(28) Elías, A. L.; Perea-López, N.; Castro-Beltrán, A.; Berkdemir, A.; Lv, R.; Feng, S.; Long, A. D.; Hayashi, T.; Kim, Y. A.; Endo, M.; Gutiérrez, H. R.; Pradhan, N. R.; Balicas, L.; Mallouk, T. E.; López-Urías, F.; Terrones, H.; Terrones, M. Controlled Synthesis and Transfer of Large-Area WS2 Sheets: From Single Layer to Few Layers. *ACS Nano* **2013**, *7*, 5235−5242.

(29) Liu, H. F.; Wong, S. L.; Chi, D. Z. CVD Growth of MoS2-Based Two-Dimensional Materials. *Chem. Vap. Deposition* **2015**, *21*, 241−259.

(30) Ji, Q.; Zhang, Y.; Gao, T.; Zhang, Y.; Ma, D.; Liu, M.; Chen, Y.; Qiao, X.; Tan, P.-H.; Kan, M.; Feng, J.; Sun, Q.; Liu, Z. Epitaxial Monolayer MoS2 on Mica with Novel Photoluminescence. *Nano Lett.* **2013**, *13*, 3870−3877.

(31) Bertuch, A.; Sundaram, G.; Saly, M.; Moser, D.; Kanjolia, R. Atomic Layer Deposition of Molybdenum Oxide Using Bis(tert-Butylimido)bis(dimethylamido) Molybdenum. *J. Vac. Sci. Technol., A* **2014**, *32*, 01A119.

(32) Vos, M. F. J.; Macco, B.; Thissen, N. F. W.; Bol, A. A.; Kessels, W. M. M. Atomic Layer Deposition of Molybdenum Oxide from (NtBu)2(NMe2)2Mo and O2 Plasma. *J. Vac. Sci. Technol., A* **2016**, *34*, 01A103.

(33) Zhan, Y.; Liu, Z.; Najmaei, S.; Ajayan, P. M.; Lou, J. Large-Area Vapor-Phase Growth and Characterization of MoS(2) Atomic Layers on a SiO(2) Substrate. *Small* **2012**, *8*, 966−971.

(34) Haas, A. The Chemistry of Silicon-Sulfur Compounds. *Angew. Chem., Int. Ed. Engl.* **1965**, *4*, 1014−1023.

(35) Carlson, R. O.; Hall, R. N.; Pell, E. M. Sulfur in Silicon. *J. Phys. Chem. Solids* **1959**, *8*, 81−83.

(36) Nikam, R. D.; Lu, A. Y.; Sonawane, P. A.; Kumar, U. R.; Yadav, K.; Li, L. J.; Chen, Y. T. Three-Dimensional Heterostructures of MoS2 Nanosheets on Conducting MoO2 as an Efficient Electrocatalyst to Enhance Hydrogen Evolution Reaction. *ACS Appl. Mater. Interfaces* **2015**, *7*, 23328−23335.

(37) Spevack, P. a.; McIntyre, N. S. A Raman and XPS Investigation of Supported Molybdenum Oxide Thin Films. 2. Reactions with Hydrogen Sulfide. *J. Phys. Chem.* **1993**, *97*, 11031−11036.

DOI: 10.1021/acs.chemmater.6b03951
Chem. Mater. XXXX, XXX, XXX−XXX

(38) Shi, Y.; Huang, J.-K.; Jin, L.; Hsu, Y.-T.; Yu, S. F.; Li, L.-J.; Yang, H. Y. Selective Decoration of Au Nanoparticles on Monolayer MoS2 Single Crystals. *Sci. Rep.* **2013**, *3*, 1839.
(39) Kibsgaard, J.; Chen, Z.; Reinecke, B. N.; Jaramillo, T. F. Engineering the Surface Structure of MoS2 to Preferentially Expose Active Edge Sites for Electrocatalysis. *Nat. Mater.* **2012**, *11*, 963−969.
(40) Ahn, C.; Lee, J.; Kim, H. U.; Bark, H.; Jeon, M.; Ryu, G. H.; Lee, Z.; Yeom, G. Y.; Kim, K.; Jung, J.; Kim, Y.; Lee, C.; Kim, T. Low-Temperature Synthesis of Large-Scale Molybdenum Disulfide Thin Films Directly on a Plastic Substrate Using Plasma-Enhanced Chemical Vapor Deposition. *Adv. Mater.* **2015**, *27*, 5223−5229.
(41) Zhang, R.; Li, Y.; Qi, J.; Gao, D. Ferromagnetism in Ultrathin MoS2 Nanosheets: From Amorphous to Crystalline. *Nanoscale Res. Lett.* **2014**, *9*, 586.
(42) Lee, C.; Yan, H.; Brus, L.; Heinz, T.; Hone, J.; Ryu, S. Anomalous Lattice Vibrations of Single-and Few-Layer MoS2. *ACS Nano* **2010**, *4*, 2695−2700.
(43) Zhang, Y.; Zhang, Y.; Ji, Q.; Ju, J.; Yuan, H.; Shi, J.; Gao, T.; Ma, D.; Liu, M.; Chen, Y.; Song, X.; Hwang, H. Y.; Cui, Y.; Liu, Z. Controlled Growth of High-Quality Monolayer WS 2 Layers on Sapphire. *ACS Nano* **2013**, *7*, 8963−8971.
(44) Amani, M.; Lien, D.-H.; Kiriya, D.; Xiao, J.; Azcatl, A.; Noh, J.; Madhvapathy, S. R.; Addou, R.; KC, S.; Dubey, M.; Cho, K.; Wallace, R. M.; Lee, S.-C.; He, J.-H.; Ager, J. W.; Zhang, X.; Yablonovitch, E.; Javey, A. Near-Unity Photoluminescence Quantum Yield in MoS2. *Science* **2015**, *350*, 1065−1068.
(45) Amani, M.; Burke, R. A.; Ji, X.; Zhao, P.; Lien, D.-H.; Taheri, P.; Ahn, G. H.; Kirya, D.; Ager, J. W.; Yablonovitch, E.; Kong, J.; Dubey, M.; Javey, A. High Luminescence Efficiency in MoS2 Grown by Chemical Vapor Deposition. *ACS Nano* **2016**, *10*, 6535.

DOI: 10.1021/acs.chemmater.6b03951
Chem. Mater. XXXX, XXX, XXX−XXX